A Self-Nulling Single-Layer Dual-Mode Microstrip Patch Antenna for Grating Lobe Reduction

Zabed Iqbal, *Student Member, IEEE,* Tanzeela Mitha, *Student Member, IEEE,* and Maria Pour, *Senior Member, IEEE*

***Abstract*— A single-layer, dual-mode microstrip patch antenna with self-nulling patterns is proposed. The antenna consists of a circular microstrip patch antenna, surrounded by a shorted concentric ring patch, exciting the TM_{11} and TM_{21} modes, respectively. Adaptive radiation patterns with self-scanning and nulling capabilities are realized by concomitantly exciting these two modes. To attain the mode purity, four symmetrical arc slits, inspired by the surface current distribution of the TM_{21} mode, as well as two horizontal slits are placed in the ring patch. For the miniaturization purpose, the circular patch is loaded by three vertical slits. A prototype of the proposed antenna is fabricated and tested. The measured results are in good agreement with the simulation results. To showcase the effectiveness of the proposed self-nulling dual-mode antenna, it is employed as an antenna element in a linear scanning array with element spacing greater than one-wavelength to reduce its unwanted grating lobes.**

***Index Terms*— Circular microstrip patch, ring patch, mode purity, phased array;**

I. Introduction

RECONFIGURABLE and adaptive antennas have been extensively researched in the past decade due to their ability to improve the quality, coverage and efficiency of the wireless communication systems [1]-[10]. Based on the application, the antenna can be designed to operate as frequency-reconfigurable [2], [3], polarization-reconfigurable [4], [5], pattern-reconfigurable [6], [7], or any combination of the aforementioned diversities [8]-[10]. The pattern-reconfigurable antennas have the ability to reduce unwanted interference from noisy sources, improve gain, and increase the coverage area by redirecting the main beam in the desired direction. A wide variety of the pattern-reconfigurable antennas is available in the literature [11]-[13]. Among them, the microstrip patch antennas are popularly used as they are light weight, low-profile, inexpensive, and can support different modes with distinct radiation patterns. In particular, compact multi-mode antennas consisting of circular microstrip antennas and short-circuited ring patches have been reported in [14]-[18] that could potentially excite different modes and produce independent radiation patterns at the same frequency. However, these multi-mode patches require either multiple stacked substrate layers or a complicated feeding network with multiple coaxial probes to excite the higher order modes.

In this paper, a new single-layer, compact, dual-mode concentric circular patch antenna with adaptive radiation patterns is introduced, which requires only one probe for each mode that would relax the design of its feeding network. The central circular patch and the concentric short-circuited ring patch of the proposed antenna excite the TM_{11} and TM_{21} modes, respectively, at the frequency of 10 GHz. Furthermore, the antenna is capable of generating relatively pure TM_{11} and TM_{21} radiation patterns with low cross polarization by implementing proper arc slits, inspired by the current distribution of the TM_{21} mode, as well as vertical and horizontal slits for elongating the current path and further improving the mode purity. The numerical results, carried out in HFSS [19], are validated through fabricating and testing a prototype antenna in practice. To show the effectiveness of the proposed dual-mode antenna with self-scanning and nulling capabilities, it is used as an antenna element in a linear scanning phased array with large element spacing to reduce its grating lobes.

II. Antenna Design

The geometry of the proposed dual-mode antenna is illustrated in Fig. 1, where the top and side views are presented. The antenna is printed on the Roger RT/duroid 5880LZ substrate with the relative dielectric constant of 1.96 and a height of h=1.27 *mm*. The antenna is composed of a circular disc in the center with a radius of R_1, exciting the TM_{11} mode, and a concentric shorted ring patch encompassing the circular disc, exciting the TM_{21} mode. The respective inner and outer radii of the ring are denoted by b and a in Fig. 1(b). Three vertical slits are cut on the circular disc patch, which are mainly used to miniaturize the disc by elongating the current path of the TM_{11} mode. These slits are equally spaced and symmetrically positioned with respect to the physical center of the antenna. The spacing between the two successive vertical slits is d_v. Detailed structure of the concentric ring patch is depicted in Fig. 1(b). To facilitate the mode purity, four symmetrical arc-shaped slits are etched on the ring patch, which are inspired by the current distribution of the TM_{21} mode in a ring patch. The minimum distance of the arc slits from the center of the disc is d_a. Each arc slit is curved as per an outer

Manuscript received on March xx, 2020. This work was supported in part by the National Science Foundation (NSF) CAREER Award no. ECCS-1653915 and the Alabama Graduate Research Scholars Program (GRSP) funded through the Alabama Commission for Higher Education and administered by the Alabama EPSCoR.

The authors are with the Department of Electrical and Computer Engineering, The University of Alabama in Huntsville, Huntsville, AL 35899 USA (e-mail: zi0003@uah.edu; tm0078@uah.edu; maria.pour@uah.edu).

circle of radius R_a as shown in Fig. 1(b). The arc is defined by of its angle α and the width w_a. To further improve the mode purity of the TM_{11} mode by suppressing its orthogonal mode, two horizontal slits are symmetrically loaded on the ring patch with width w_h and length l_h, each located at a distance d_h from the center. Finally, 16 metallic vias with a diameter of v_d are inserted through the substrate to short circuit the inner edge of the ring patch to the ground plane, which will help improve the isolation between the two modes. The proposed dual-mode antenna is fed by two coaxial probes, denoted by p_1 and p_2 in Fig. 1. The location of the p_1 and p_2 probes are offset from the center by distance of f_1 and f_2, respectively. The final values of the design parameters are given in Table 1.

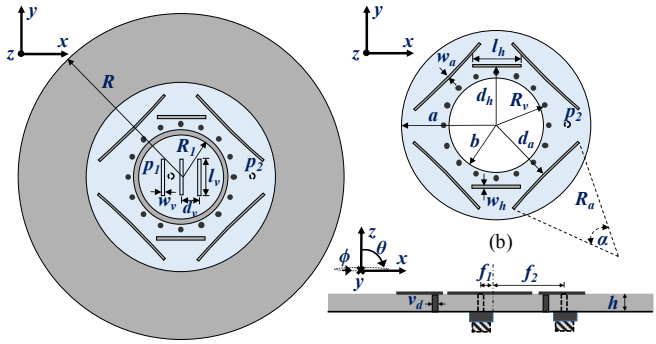

Fig. 1. Geometry of the dual-mode circular microstrip patch antenna operating at the TM_{11} and TM_{21} modes, where R_1 is the radius of the TM_{11} patch, and a and b are the outer and inner radii of TM_{21} ring patch, respectively; p_1 and p_2 represent probe locations along the x-axis. (a) Top view (b) TM_{21} ring patch (c) side view; ($\alpha = 9.33°$).

TABLE I: GEOMETRICAL PARAMETERS OF THE PROPOSED ANTENNA

Param.	Value (mm)	Param.	Value (mm)
R_1	5.00	d_v	2.20
a	11.56	w_h	0.25
b	5.84	l_h	5.80
R	20.00	d_h	7.40
h	1.27	R_a	55.00
w_v	0.25	w_a	0.20
l_v	4.40	d_a	8.15
R_v	6.40	f_1	1.10
v_d	0.40	f_2	8.97

III. FULL-WAVE NUMERICAL RESULTS

The antenna shown in Fig. 1 was full-wave analyzed using ANSYS HFSS 18.0. The simulated scattering parameters of the antenna are shown in Fig. 2, where S_{12} or S_{21} represents the mutual coupling between the TM_{11} and TM_{21} modes and the S_{11} and S_{22} are the reflection coefficients of the ports exciting the TM_{11} and TM_{21} modes, respectively. Interestingly enough, the mutual coupling of the dual-mode antenna is around -28 dB at the frequency of 10 GHz. To assess the mode purity, proper ϕ-cuts of the radiation patterns are studied. That is, in addition to the principal planes, the diagonal plane is considered for the TM_{21} mode. The results for both modes are plotted in Fig. 3. It can be seen that the H-plane patterns are more symmetric than the E-plane ones for both modes. This is because any potential asymmetry is mainly attributed to the two probes, which are offset from the center and placed along the E-plane of $\phi = 0°$. As per Fig. 3(a), the E_θ component of the TM_{11} mode in the $\phi = 90°$ plane, which should be zero theoretically, is 17.8 dB below its counterpart component in the $\phi = 0°$ plane. This is due to the mutual coupling between the modes and the effect of unwanted higher order modes.

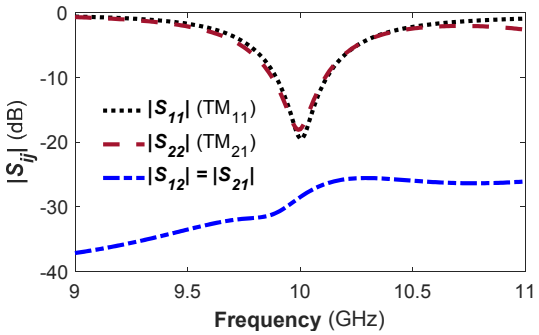

Fig. 2. Simulated scattering parameters of the dual-mode circular microstrip patch antenna shown in Fig. 1.

A same trend is observed with the TM_{21} radiation patterns shown in Fig. 3(b), when the port p_2 is excited, while the port p_1 is matched. The radiation patterns now become conical with a null at the boresight direction of $\theta = 0°$, as expected. The main beam of the TM_{21} mode is around ±37° at the principal and diagonal planes. As for the cross-polarized components, they are around 20 dB below the co-pol components, whereas in an ideal case they should be zero. This is mainly due to the small leakage current of the y-polarized TM_{11} mode, which has considerably been suppressed by the horizontal slits in the ring patch. For further clarification, the surface current distributions of the TM_{11} and TM_{21} mode of the proposed antenna are depicted in Figs. 4(a) and 4(b), respectively, and compared with the ideal current distribution [20] of the TM_{11} circular patch and TM_{21} ring patch, shown in Figs. 4(c) and 4(d). As can be seen, the current distribution of the TM_{11} mode is elongated due the three vertical slits, whereas a quite symmetrical current distribution for the TM_{21} mode is obtained in each quadrant by employing the four arc-shaped slits in the ring patch, which are inspired by the ideal current distribution of the TM_{21} mode illustrated in Fig. 4(d). Moreover, the y-polarized E-field of the orthogonal TM_{11} modes are weakened by the two horizontal slits on the TM_{21} ring patch, as shown in Fig. 4(b). As a result, the mode purity of the higher order TM_{21} and cross polarization of the fundamental TM_{11} mode are improved.

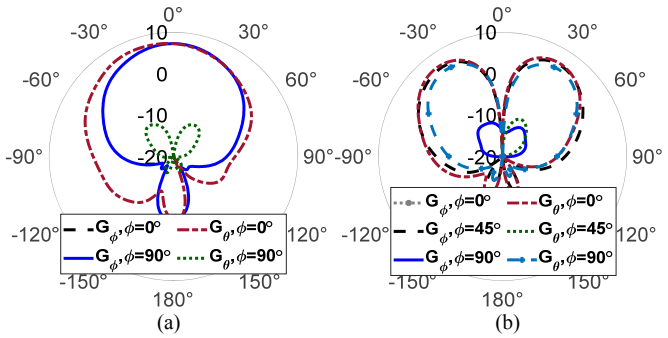

Fig. 3. Simulated gain patterns of the proposed dual-mode circular microstrip patch antenna operating at the (a) TM_{11} mode (b) TM_{21} mode at 10 GHz.

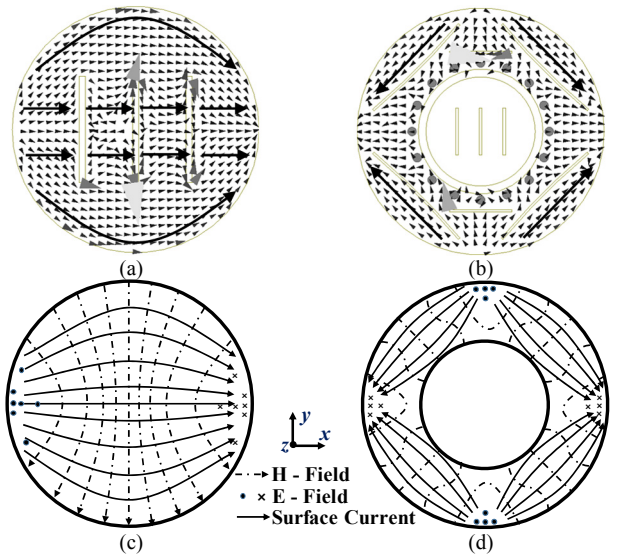

Fig. 4. Surface current distributions of the proposed antenna at the (a) TM_{11} mode (b) TM_{21} mode at 10 GHz; ideal distributions of (c) TM_{11} circular patch (d) TM_{21} ring patch.

IV. Parametric Studies

Fig. 5(a) shows the simulated gain patterns of the proposed dual-mode circular microstrip patch antenna operating at the TM_{21} mode at 10 GHz without the arc slits. As can be seen, the TM_{21} radiation patterns are distorted and the unwanted cross-pol component at the both principal and diagonal planes are as high as -3 dB. That is, E_ϕ at the H-plane ($\phi = 90°$) and E_θ at the diagonal plane ($\phi = 45°$), which should have been ideally zero, become comparable with the co-pol components. More importantly, the co-polar components no longer have right-left symmetry. Thus, the mode purity of the TM_{21} mode greatly depends on the four symmetrical arc slits, inspired by the current distribution of the mode. This will in turn facilitate containing a relatively ideal current distribution of the TM_{21} mode on the ring patch, which also helps suppress the orthogonal y-polarized TM_{11} mode in the ring patch.

In order to investigate the effect of the arc slits on the impedance matching, a parametric study is carried out in terms of the opening angle of the slits. Fig. 5(b) shows the simulated reflection coefficients as a function of frequency for different angles (α) of the arc slit. As observed, the $|S_{22}|$ is quite sensitive to α. More specifically, the resonant frequency of the TM_{21} mode can be fine-tuned to 10 GHz, when α = 9.33°. This optimal value results in good impedance matching and mode purity for both modes as per Figs. 5 and 3, respectively.

Two symmetrical horizontal slits on the TM_{21} ring patch are etched to partially block the y-polarized leakage current of the TM_{11} modes, which directly attribute to the cross-polarized component of the TM_{21} mode. To demonstrate the effect of horizontal slits on mode purity, simulated gain patterns of the proposed antenna without the horizontal slits are shown in Fig. 6(a). As expected, both unwanted cross-polarized components, i.e., E_ϕ at ϕ= 90° and E_θ at the ϕ = 45°, increase. Another parametric study is carried out to understand the miniaturization effects of the horizontal slits on the TM_{21} patch, whose results are shown in Fig. 6(b) for different lengths (l_h) of the slits. As observed, the longer the slits, the lower the resonant frequency of the TM_{21} mode and with l_h=5.8mm, about 4.5% size reduction is realized compared to the TM_{21} patch without any horizontal slits. It should be noted that the vertical slits in the TM_{11} patch are mainly used to miniaturize the patch, leading to about 20.4% size reduction compared to a conventional patch.

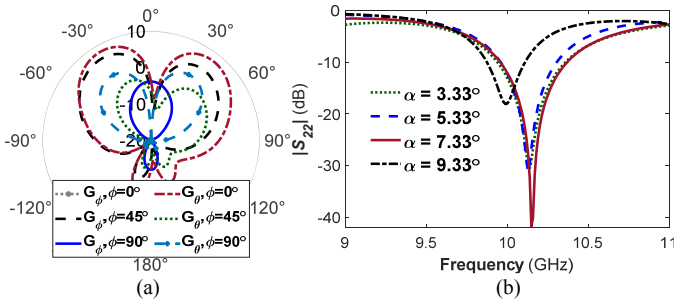

Fig. 5. Simulated (a) gain patterns without arc slits (b) scattering parameters for different arc slit lengths of the proposed antenna at the TM_{21} mode at 10 GHz.

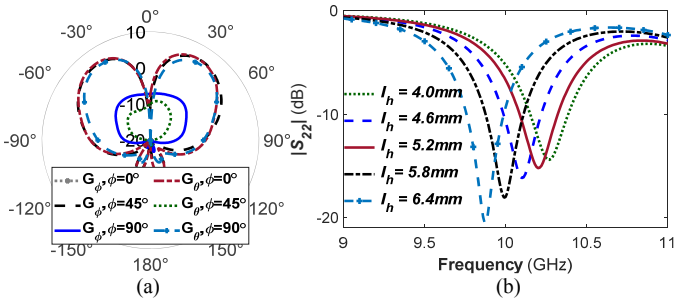

Fig. 6. Simulated (a) gain patterns without horizontal slits (b) scattering parameters of the proposed antenna at the TM_{21} mode at 10 GHz.

V. Self-Scanning and Nulling

The dual-mode circular microstrip antenna under study exhibits unique self-scanning and nulling [21] properties through its radiation characteristics. The main beam scanning direction and null position of the antenna can be controlled by the relative mode content factor, which is the excitation ratio of the TM_{21} mode to the TM_{11} mode, denoted herein by A_{21}, a complex number in general. The scanning/nulling capabilities of the dual-mode antenna are shown in Fig. 7, through both simulation and measurement, with a -90° phase shift between the modes. As observed, the main beam further scans towards positive elevation angles, as $|A_{21}|$ increases. Moreover, a full null is formed when $|A_{21}|$=1. By only reversing the polarity of the phase shift between the probes, one can change the beam scanning/nulling directions to the opposite sides, whose results are omitted here for brevity.

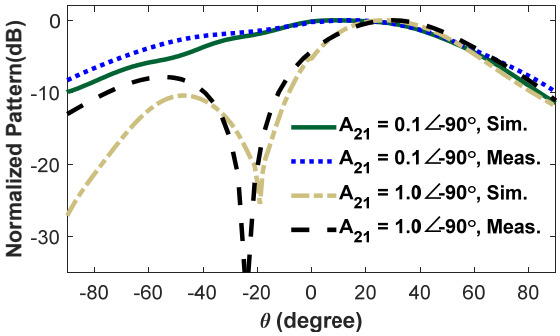

Fig. 7. Simulated and measured beam scanning capabilities of the proposed antenna shown in Fig. 1 for different A_{21}.

VI. Experimental Results

The proposed dual-mode microstrip patch antenna with its final dimensions listed in Table 1 is fabricated and measured. Two SMA connectors are used to excite the antenna. To excite one mode at a time, the probe of the other mode is matched with a 50Ω load. A photograph of the fabricated antenna is shown in Fig. 8(a). The measured and simulated $|S_{ij}|$ response of the proposed antenna is depicted in Fig. 8(b). Both the simulated and measured $|S_{11}|$ and $|S_{22}|$ are well below -10 dB at 10 GHz. The small frequency shit between simulated and measured results is mainly due to the fabrication errors and slightly different solder joints for each mode. There is good agreement between simulated and measured transmission coefficients $|S_{12}|$, both of which are below -25 dB at 10 GHz. The radiation patterns of the fabricated antenna are measured in the spherical near-field anechoic chamber of the University of Alabama in Huntsville at 10 GHz. The measured results are compared with the simulated ones in Figs. 9 and 10 for the TM_{11} and TM_{21} modes, respectively, which are in good agreement. As expected, broadside radiation patterns are obtained for the fundamental TM_{11} mode as shown in Fig. 9, and conical patterns with a -20 dB null at the $\theta = 0^{o}$ are achieved for the higher order TM_{21} mode, as per Fig. 10. The split main beam direction is around $\theta = \pm 35°$ for the TM_{21} mode in both of simulation and measurement.

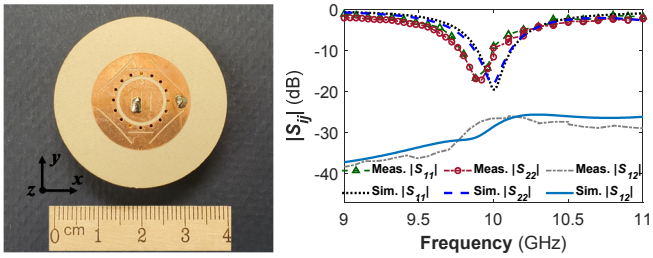

(a) (b)

Fig. 8. (a) Top view and (b) simulated and measured s-parameters of the proposed antenna.

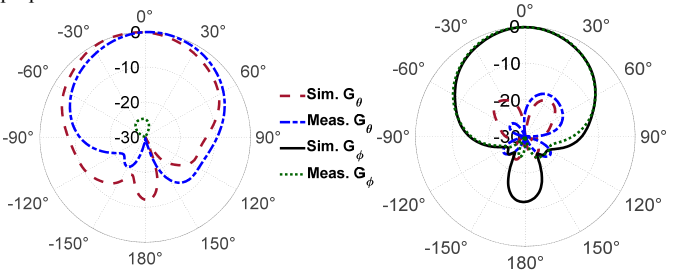

(a) (b)

Fig. 9. Normalized measured and simulated radiation patterns of the proposed antenna TM_{11} mode (a) $\phi = 0°$, and (b) $\phi = 90°$ at 10 GHz.

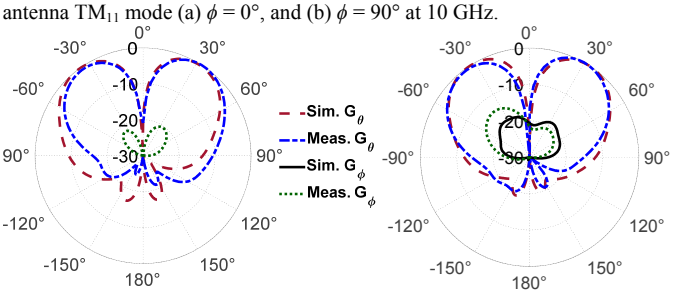

(a) (b)

Fig. 10. Normalized measured and simulated radiation patterns of the proposed antenna TM_{21} mode (a) $\phi = 0°$ and (b) $\phi = 90°$ at 10 GHz.

VII. Application: Grating Lobe Reduction

To design a low-cost scanning phased array antenna with high gain, researchers often use reduced numbers of antenna elements while keeping the aperture size as large as possible. To this end, large element spacing between the antenna elements is required. However, element spacing more than half a wavelength in the linear arrays generates grating lobes. Recently, the authors utilized the analytical results of a stacked dual-mode circular patch antenna in scanning phased array antennas in [22], [23] to reduce grating lobes with the element separation significantly larger than half a wavelength.

Now, in order to examine the grating lobe reduction capability of the proposed single-layer, dual-mode antenna element, a synthesized simulated and measured radiation patterns of a seven-element linear phased array is shown in Fig. 11 as a representative example, for the scan angle of $\theta_o = -20°$, when the element spacing is 1.25 times the free-space wavelength. With such large element spacing, the mutual coupling is small and thus the total radiation pattern for the array is synthesized by directly multiplying the element radiation patterns with the array factor. In conventional single-mode elements, the grating lobe almost as large as the main lobe appears at $\theta_o = +30°$. Interestingly enough, by adopting the proposed antenna element, the grating lobes are lowered to below -23.5 dB in both simulated and measured cases, as shown in Fig. 11. The main reason behind the grating lobe reduction is that the proposed dual-mode element is radiation-matched with the scanned beam of the array and it does possess a null near the grating lobe. The gain of the single-mode and dual-mode seven-element arrays are 16.25 dBi and 17.2 dBi, respectively for the scan angle of $\theta_o = -20°$. Interestingly enough, the overall gain drop in the dual-mode seven-element array antenna is less than that of its counterpart single-mode array, especially for the medium scan angles.

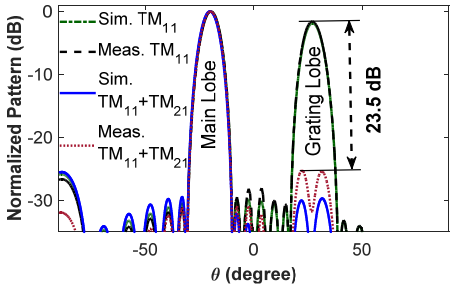

Fig. 11. Normalized simulated and measured radiation patterns of a 7-element linear phased array consisting of the proposed dual-mode antenna element while scanning at θ_o=-20° for the element spacing of $1.25\lambda_o$.

VIII. Conclusion

A dual-mode, single-layer, microstrip patch antenna, consisting of a circular patch and a concentric shorted ring was proposed. The antenna exhibited excellent mode purity in the fundamental TM_{11} mode. To generate pure TM_{21} mode, sixteen shorted pins, four symmetrical arc slits, and two horizontal slits were adopted in the ring patch. A self-scanning and nulling radiation pattern was realized by properly exciting both modes simultaneously. The antenna was used as a radiation-matched base element in a linear scanning phased array with large element spacing to reduce their unwanted grating lobes.

REFERENCES

[1] R. Haupt, M. Lanagan, "Reconfigurable antennas", *IEEE Antennas Propag. Mag.*, vol 55, pp. 49-61, Feb. 2013.

[2] H. A. Majid, M. K. A. Rahim, M. R. Hamid, and M. F. Ismail, "A compact frequency-reconfigurable narrowband microstrip slot antenna," *IEEE Antennas Wireless Propag. Lett*., vol. 11, pp. 616-619, Jun. 2012.

[3] D. Peroulis, K. Sarabandi, and L. Katehi, "Design of reconfigurable slot antennas", *IEEE Trans. Antennas Propag*., vol. 53, no. 12, pp. 645-654, Feb. 2005.

[4] B. Kim, "A novel single-feed circular microstrip antenna with reconfigurable polarization capability", *IEEE Trans. Antennas Propag*., vol.56, no. 3,pp. 630-638, Mar. 2008.

[5] P. Qin, A. Weily, Y. Guo, and C. Liang, "Polarization reconfigurable u-slot patch antenna," *IEEE Trans. Antennas Propag.,* vol. 58, no. 10 , pp. 3383-3388, Oct. 2010.

[6] W. Kang, J. Park, and Y. Yoon, "Simple reconfigurable antenna with radiation pattern", *Electron. Lett.,* vol.44, no.3, pp. 182-183, 31 Jan. 2008.

[7] S. Chen, J. Row, and K. Wong, "Reconfigurable square-ring patch antenna with pattern diversity", *IEEE Trans. Antennas Propag.,*vol. 55, no. 2, pp. 472-475, Feb. 2007.

[8] N. Nguyen-Trong, L. Hall, and C. Fumeaux, "A frequency- and polarization-reconfigurable stub-loaded microstrip patch antenna", *IEEE Trans. Antennas Propag*., vol. 63, no.11, pp. 5235-5240, Nov. 2015.

[9] P. K. Li, Z. H. Shao, Q. Wang, and Y. J. Cheng, "Frequency- and pattern-reconfigurable antenna for multistandard wireless applications", *IEEE Antennas Wireless Propag. Lett*.,vol. 14 , pp. 333-336, Sept. 2014.

[10] W. Cao, "Compact dual-band dual-mode circular patch antenna with broadband unidirectional linearly polarised and omnidirectional circularly polarised characteristics," *IET Microw. Antennas Propag.,* vol.10, no. 2, pp. 223-229, Jan. 2016.

[11] J. Ren, X. Yang, J. Yin, and Y. Yin, "A Novel Antenna with Reconfigurable Patterns Using H-Shaped Structures," *IEEE Antenna Wireless Propag. Lett*., vol.14, pp. 915-918, Dec. 2015.

[12] I. Lim and S. Lim, "Monopole-Like and Boresight Pattern Reconfigurable Antenna," *IEEE Trans. Antennas Propag.,* vol. 61 , no, 12, pp. 5854-5859, Dec. 2013.

[13] X. –S. Yang, B.-Z. Wang, W. Wu, and S. Xiao, "Yagi Patch Antenna With Dual-Band and Pattern Reconfigurable Characteristics," *IEEE Antennas Wireless Propag. Lett.*, vol. 6,, pp. 168-171, April 2007.

[14] N. Herscovici, C. Christodoulou, E. Rajo-Iglesias, O. Quevedo-Teruel, and M. Sanchez-Fernandez, "Compact multimode patch antennas for MIMO applications", *IEEE Antennas Propag. Mag.,* vol. 50, no. 2, pp. 197-205, April 2008.

[15] T. Q. Tran and S. K. Sharma, "Radiation characteristics of a multimode concentric circular microstrip patch antenna by controlling amplitude and phase of modes," *IEEE Trans. Antennas Propag*., vol. 60, no. 3, pp. 1601-1605, March 2012.

[16] Z. Zhang, S. Xiao, Y. Li, and B.-Z. Wang, "A circularly polarized multimode patch antenna for the generation of multiple orbital angular momentum modes," *IEEE Antennas Wireless Propag. Lett*., vol.16, pp. 521-524, July 2016.

[17] Y. Lin and L. Shafai, "Characteristics of concentrically shorted circular patch microstrip antennas", *IEE Proc. Microw. Antennas Propag*., vol. 137, pp. 18-24, Feb. 1990.

[18] J. Watkins, "Circular resonant structures in microstrip", *Electron. Lett*., vol. 5, no.21, pp. 524-525, Oct. 1969.

[19] *High Frequency Structure Simulator (HFSS 18.0)*. Canonsburg, PA, USA, ANSYS, 2017.

[20] R. Garg, P. Bhartia, I. J. Bahl, and A. Ittipiboon, *Microstrip Antenna Design Handbook*. Artech House, 2001.

[21] Z. Iqbal and M. Pour, "Amplitude control null steering in a multi-mode patch antenna," *Progress in Electromagnetics Research Lett*., vol. 82, pp. 107–112, 2019.

[22] Z. Iqbal and M. Pour, "Grating lobe reduction in scanning phased array antennas with large element spacing," *IEEE Trans. Antennas Propag*., vol. 66, no. 12, pp. 6965–6974, Dec. 2018.

[23] Z. Iqbal and M. Pour, "Exploiting higher order modes for grating lobe reductions in scanning phased array antennas," *IEEE Trans. Antennas Propag*., vol. 67, no. 11, pp. 7144–7149, Nov. 2019.